Chem Biol Drug Des 2014

Research Article

Synthesis, Biological Evaluation, and Molecular Simulation of Chalcones and Aurones as Selective MAO-B Inhibitors

Nicole Morales-Camilo[1], Cristian O. Salas[1,*], Claudia Sanhueza[2], Christian Espinosa-Bustos[1], Silvia Sepúlveda-Boza[2], Miguel Reyes-Parada[2,3], Fernando Gonzalez-Nilo[4], Marcos Caroli-Rezende[5] and Angélica Fierro[1,*]

[1]Departamento de Química Orgánica, Facultad de Química, Pontificia Universidad Católica de Chile, Santiago de Chile 702843, Chile
[2]Escuela de Medicina, Facultad de Ciencias Médicas, Universidad de Santiago, Casilla 442, Correo 2, Santiago, Chile
[3]Facultad de Ciencias de la Salud, Universidad Autónoma de Chile, Santiago 8910124, Chile
[4]Universidad Andrés Bello, Facultad de Ciencias Biológicas, Centro de Bioinformática y Biología Integrativa, Santiago 8370146, Chile
[5]Departamento de Química de los Materiales, Facultad de Química y Biología, Universidad de Santiago de Chile, Casilla 40, Correo 33, Santiago 9170022, Chile
**Corresponding authors: Angélica Fierro, afierroh@uc.cl; Cristian O. Salas, cosalas@uc.cl*

A series of chalcones and aurones were synthesized and evaluated *in vitro* as monoamine oxidase inhibitors (MAOi). Our results show that aurones, which had not been previously reported as MAOi, are MAO-B inhibitors. Thus, both families inhibited selectively the B isoform of MAO in the micromolar range, offering novel scaffolds for the design of new and potent MAO inhibitors. The main structural requirements for their activity were characterized with the aid of 3D-QSAR and docking studies.

Key words: aurones, chalcones, molecular modeling, monoamine oxidase inhibitors, QSAR

Received 7 July 2014, revised 11 September 2014 and accepted for publication 12 October 2014

Chalcones and aurones are natural and synthetic compounds whose recorded actions on biological targets make them interesting scaffolds for the design of potential therapeutic agents (1–7). Examples of the former are xanthohumol and cardamonin (Figure 1), of interest as anticancer (8–13) and antibacterial agents (14), and preventing platelet aggregation (15). Aurones such as sulfuretin are known to suppress inflammation and oxidative stress (16–18) and have anticancer properties (19,20). Aureusidin has shown antioxidant activity (21), and 4-chloroaurone, isolated from a marine source, *Spatoglossum variabile,* has been modified to obtain compounds with potent antibacterial activity (22).

Among the many pharmacologically interesting applications of chalcones, their potential as monoamine oxidase inhibitors (MAOi) has been recently described by different groups (23–26). MAO is a flavoprotein involved in the degradation of a wide range of endogenous and exogenous monoamines, including the neurotransmitters serotonin, dopamine, and noradrenaline (27). The enzyme exists in two isoforms, MAO-A and MAO-B (28), which are bound to the mitochondrial outer membrane as dimers (29,30). Both proteins have similar structures and molecular weights (70% amino acid sequence identity), but differ in their selectivity for substrates and inhibitors (27). As MAO-A and MAO-B modulate the levels of key signaling molecules, inhibitors of these enzymes have been developed as drugs for the treatment of neuropsychiatric and neurodegenerative disorders (26). Thus, reversible MAO-A inhibitors such as moclobemide (31) are currently used as effective antidepressants, whereas MAO-B inhibitors are useful in the treatment of Parkinson′s disease (26,32). The latter indication is especially relevant in elderly patients with Parkinson′s disease, as it has been shown that brain MAO-B levels increase with age, resulting in an acceleration of the neurodegenerative processes (33,34). Therefore, as the detailed chemical structures of MAO-A and MAO-B are available, this information provides new possibilities for the development of promising novel inhibitors (35–37).

Following previous reports on the activity of chalcones as MAOi, we decided to investigate a series of synthetic substituted chalcones. In addition, our study included for the first time a series of aurones, in order to explore their pharmacological activity and to compare their putative MAOi activity with that of the related chalcones. In spite of some reports describing their therapeutic potential (6,28), aurones have not yet been reported as MAOi.

The evaluation of a total of 16 compounds, 8 chalcones, and 8 aurones was followed by a selection of the most

 doi: 10.1111/cbdd.12458

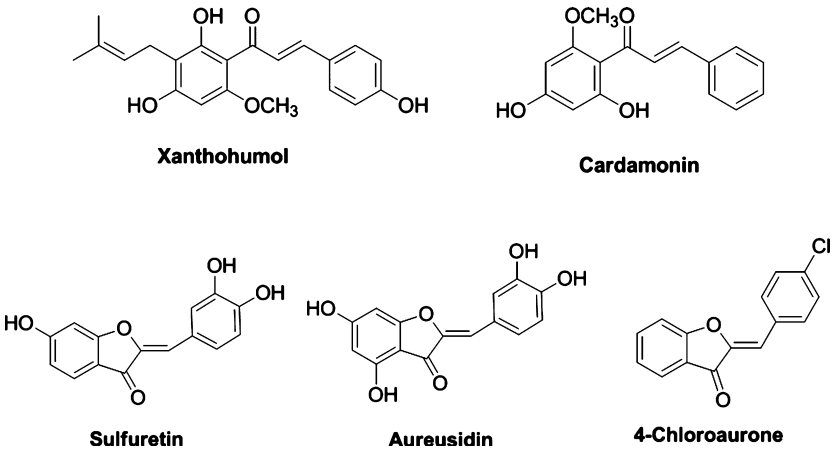

Figure 1: Chemical structures of bioactive chalcone and aurone derivatives.

active compounds of both sets, and by 3D-QSAR and docking studies, to identify the principal structural features that might be responsible for their activity.

Experimental

Melting points were determined on a Reichert–Thermogeräte–Kofler apparatus and are uncorrected. Infrared spectra were recorded on a Bruker Model Vector 22 spectrophotometer (Bruker Optik GmbH, Bremen, Germany) using KBr disks. Nuclear magnetic resonance spectra were recorded on a Bruker AM-400 apparatus using $CDCl_3$ solutions containing TMS as internal standard. HPLC–MS experiments were performed on a Thermo Scientific Exactive Orbitrap MS, Bremen, Germany. Mass spectra were obtained on a Hewlett-Packard (HP) 5988A spectrometer. Thin-layer chromatography (TLC) was performed using Merck GF-254 type 60 silica gel. Column chromatography was carried out using Merck silica gel 60 (70–230 mesh). 2,5- and 2,6-dihydroxyacetophenones and the substituted aldehydes were purchased from Sigma-Aldrich, St. Louis, MO, USA. The 2-hydroxy-6-methoxyacetophenone and 2-hydroxy-5-methoxyacetophenone were prepared by methylation of commercial 2,6-dihydroxyacetophenone and 2,5-dihydroxyacetophenone with methyl iodide, following a reported procedure (38).

General synthetic procedure to obtain chalcones (3a–3h)

To a stirred solution of 2-hydroxy-5-methoxy- or of the 2-hydroxy-6-methoxyacetophenone (**2a** or **2b**) (0.01 mol) and the appropriate aldehyde (0.02 mol) in EtOH (30 mL) was added 50% aqueous KOH (30 mL). The mixture was stirred for 12 h at room temperature. The reaction mixture was then made acid with dilute HCl, and the precipitated solid was filtered and washed with cold water. The obtained yellow-orange solid was purified by flash column chromatography using CH_2Cl_2 as eluent. In this way, the following chalcones were prepared.

(E)-3-(2,5-Dimethoxyphenyl)-1-(2-hydroxy-6-methoxyphenyl)prop-2-en-1-one (3a)

Orange solid, yield 35%, mp: 134.3–135.9 °C. ^{1}H NMR (400 MHz, $CDCl_3$) δ ppm: 3.81 (s, 3H), 3.87 (s, 3H), 3.94 (s, 1H), 6.42 (d, J = 8.2 Hz, 1H), 6.61 (d, J = 8.3 Hz, 1H), 6.87 (d, J = 9.0 Hz, 1H), 6.93 (d, J = 2.9, 9.0 Hz, 1H), 7.15 (d, J = 2.8 Hz, 1H), 7.35 (t, J = 8.3 Hz, 1H), 7.90 (d, J = 15.7 Hz, 1H), 8.12 (d, J = 15.7 Hz, 1H), 13.19 (s, 1H). ^{13}C NMR (101 MHz; $CDCl_3$) δ ppm: 55.8, 55.9, 56.1, 101.5, 110.9, 112.1, 112.4, 113.8, 116.8, 125.0, 128.3, 135.7, 138.2, 153.4, 153.5, 161.0, 164.8, 194.8. IR (KBr, cm^{-1}): 2932, 2821, 1605, 1497, 1439, 1220. MS (ESI): 314.0 ($C_{18}H_{18}O_5$ [M + H]$^+$). HRMS-ES (m/z): [M + H]$^+$ calcd for $C_{18}H_{18}O_5$, 314.1154; found, 315.1222.

(E)-1-(2-Hydroxy-6-methoxyphenyl)-3-(2,4,5-trimethoxyphenyl)prop-2-en-1-one (3b)

Orange solid, yield 74%, mp: 133.6–133.8 °C [lit. 132–133 °C (39)] ^{1}H NMR (400 MHz, $CDCl_3$) δ ppm: 3.89 (s, 3H), 3.91 (s, 3H), 3.94 (s, 3H), 3.95 (s, 3H), 6.42 (d, J = 8.2 Hz, 1H), 6.52 (s, 1H), 6.61 (d, J = 8.3 Hz 1H), 7.12 (s, 1H), 7.34 (t, J = 8.3 Hz, 1H), 7.83 (d, J = 15.6 Hz, 1H) 8.16 (d, J = 15.7 Hz, 1H), 13.33 (s, 1H). ^{13}C NMR (101 MHz; $CDCl_3$) δ ppm: 55.8, 56.1, 56.4, 56.5, 96.9, 101.5, 110.9, 111.5, 112.2, 116.0, 125.4, 135.4, 138.6, 143.2, 152.5, 154.8, 160.8, 164.8, 194.5. IR (KBr, cm^{-1}): 2937, 2785, 1659, 1288, 1218, 1027. MS (ESI): 344.0 ($C_{19}H_{20}O_6$ [M + H]$^+$). HRMS-ES (m/z): [M + H]$^+$ calcd for $C_{19}H_{20}O_6$, 344.1260; found, 345.1328.

(E)-3-(2,3-Dimethoxyphenyl)-1-(2-hydroxy-6-methoxyphenyl)prop-2-en-1-one (3c)

Orange solid, yield 99%, mp: 112.0–114.1 °C [lit. 115–116 °C (39)] ^{1}H NMR (400 MHz, $CDCl_3$) δ ppm: 3.89 (s, 3H), 3.90 (s, 3H), 3.93 (s, 3H), 6.42 (d, J = 8.3 Hz, 1H), 6.61 (d, J = 8.3 Hz, 2H), 6.96 (d, J = 8.0 Hz, 2H), 7.09 (t, J = 8.0 Hz, 1H), 7.24 (d, J = 7.8 Hz, 1H), 7.35 (t, J = 8.3 Hz, 1H), 7.92 (d, J = 15.8 Hz, 1H), 8.11 (d, J = 15.8 Hz, 1H) 13.17 (s, 1H). ^{13}C NMR (101 MHz;

$CDCl_3$) δ ppm: 55.9, 56.0, 61.3, 101.5, 110.9, 112.1, 113.9, 119.8, 124.2, 128.9, 129.5, 135.8, 137.8, 149.0, 153.2, 161.0, 164.9, 194.7. IR (KBr, cm^{-1}): 2938, 2835, 1632, 1561, 1240, 1093. MS (ESI): 314.0 ($C_{18}H_{18}O_5$ $[M + H]^+$). HRMS-ES (m/z): $[M + H]^+$ calcd for $C_{18}H_{18}O_5$, 314.1154; found, 315.1216.

(E)-3-(4-Bromo-2,5-dimethoxyphenyl)-1-(2-hydroxy-6-methoxyphenyl)prop-2-en-1-one (3d)

Orange solid, yield 93%, mp: 188.3–188.9 °C. ^1H NMR (400 MHz, $CDCl_3$) δ ppm: 3.88 (s, 3H), 3.90 (s, 3H), 3.93 (s, 3H) 6.43 (d, J = 8.2 Hz, 1H), 6.62 (dd, J = 0.6, 8.3 Hz, 1H), 7.11 (s, 1H), 7.15 (s, 1H), 7.36 (t, J = 8.3 Hz, 1H), 7.93 (d, J = 15.7 Hz, 1H) 8.02 (d, J = 15.7 Hz, 1H), 13.14 (s, 1H). ^{13}C NMR (101 MHz; $CDCl_3$) δ ppm: 55.8, 56.3, 56.9, 101.6, 111.0, 112.1, 112.2, 114.7, 117.0, 124.1, 128.7, 135.9, 137.6, 150.2, 153.4, 160.9, 164.9, 194.6. IR (KBr, cm^{-1}): 2961, 2834, 1631, 1561, 1237, 1217. MS (ESI): 393.0 ($C_{18}H_{17}O_5Br$ $[M + H]^+$).

(E)-3-(2,5-Dimethoxyphenyl)-1-(2-hydroxy-5-methoxyphenyl)prop-2-en-1-one (3e)

Orange solid, yield 35%, mp: 156.8–158.1 °C. ^1H NMR (400 MHz, $CDCl_3$) δ ppm: 3.82 (s, 3H), 3.83 (s, 3H), 3.88 (s, 3H), 3.94 6.88 (d, J = 8.9 Hz, 1H), 6.96 (d, J = 8.9 Hz, 2H), 7.09–7.17 (m, 2H), 7.35 (d, J = 3.0 Hz, 1H), 7.66 (d, J = 15.6 Hz, 1H), 8.17 (d, J = 15.7 Hz, 1H), 12.46 (s, 1H). ^{13}C NMR (101 MHz; $CDCl_3$) δ ppm: 55.9, 56.0, 56.1, 112.5, 112.9, 114.3, 117.6, 119.2, 119.8, 121.0, 123.7, 124.2, 141.0, 151.7, 153.5, 153.6, 157.9, 193.9. IR (KBr, cm^{-1}): 2942, 2835, 1617, 1550, 1285, 1238. MS (ESI): 314.0 ($C_{18}H_{18}O_5$ $[M + H]^+$). HRMS-ES (m/z): $[M + H]^+$ calcd for $C_{18}H_{18}O_5$, 314.1154; found, 315.1210.

(E)-1-(2-Hydroxy-5-methoxyphenyl)-3-(2,4,5-trimethoxyphenyl)prop-2-en-1-one (3f)

Orange solid, yield 61%, mp: 159.3–161.0 °C [lit. 162–163 °C (39)]. ^1H NMR (400 MHz, $CDCl_3$) δ ppm: 3.84 (s, 3H), 3.92 (s, 3H), 3.93 (s, 3H), 3.96 (s, 3H), 6.53 (s, 1H), 6.97 (d, J = 9.0 Hz, 1H), 7.13 (m, 2H), 7.40 (d, J = 2.8 Hz, 1H), 7.56 (d, J = 15.5 Hz, 1H), 8.21 (d, J = 15.5 Hz, 1H), 12.59 (s, 1H). ^{13}C NMR (101 MHz; $CDCl_3$) δ ppm: 56.5, 56.6, 56.7, 57.1, 97.1, 112.4, 113.9, 115.6, 118.4, 119.5, 120.5, 123.3, 141.5, 143.8, 151.9, 153.5, 155.6, 158.2, 194.2. IR (KBr, cm^{-1}): 2945, 2836, 1557, 1238, 1267, 1172, 1022. MS (ESI): 344.0 ($C_{19}H_{20}O_6$ $[M + H]^+$). HRMS-ES (m/z): $[M + H]^+$ calcd for $C_{19}H_{20}O_6$, 344.1260; found, 345.1331.

(E)-3-(2,3-Dimethoxyphenyl)-1-(2-hydroxy-5-methoxyphenyl)prop-2-en-1-one (3g)

Orange solid, yield 34%, mp: 159.5–160.1 °C [lit. 102–103 °C (39)]. ^1H NMR (400 MHz, $CDCl_3$) δ ppm: 3.84 (s, 3H), 3.91 (s, 3H), 3.92 (s, 3H), 6.99 (t, J = 8.5 Hz, 2H), 7.09–7.18 (m, 2H), 7.27 (d, J = 9.8 Hz, 1H), 7.36 (d, J = 2.9 Hz, 1H), 7.71 (d, J = 15.6 Hz, 1H), 8.19 (d, J = 15.6 Hz, 1H), 12.42 (s, 1H). ^{13}C NMR (101 MHz; $CDCl_3$): δ ppm: 56.3, 56.5, 61.7, 113.2, 115.0, 119.8, 120.1, 120.5 (2C), 122.2, 124.4 (2C), 124.7, 129.2, 141.1, 152.1, 158.4, 194.2. IR (KBr, cm^{-1}): 2943, 2835, 1573, 1486, 1278, 1175. MS (ESI): 314.0 ($C_{18}H_{18}O_5$ $[M + H]^+$). HRMS-ES (m/z): $[M + H]^+$ calcd for $C_{18}H_{18}O_5$, 314.1154; found, 315.1222.

(E)-3-(4-Bromo-2,5-dimethoxyphenyl)-1-(2-hydroxy-5-methoxyphenyl)prop-2-en-1-one (3h)

Orange solid, yield 42%, mp: 159.9–160.3 °C. ^1H NMR (400 MHz, $CDCl_3$) δ ppm: 3.83 (s, 3H), 3.89 (s, 3H), 3.91 (s, 3H), 6.96 (d, J = 9.0 Hz, 1H), 7.04–7.18 (m, 3H), 7.35 (d, J = 2.8 Hz, 1H), 7.67 (d, J = 15.6 Hz, 1H), 8.06 (d, J = 15.6 Hz, 1H), 12.38 (s, 1H). ^{13}C NMR (101 MHz; $CDCl_3$) δ ppm: 56.1, 56.3, 57.0, 112.6, 113.4, 115.6, 117.0, 119.2, 119.8, 121.4, 123.3, 123.4, 140.4, 150.2, 151.6, 153.5, 157.9, 193.7. IR (KBr, cm^{-1}): 2917, 2834, 1640, 1573, 1487, 1462, 1050. MS (ESI): 393.0 ($C_{18}H_{17}O_5Br$ $[M + H]^+$). HRMS-ES (m/z): $[M + 2H]^+$ calcd for $C_{18}H_{17}O_5Br$, 392.0259; found, 395.0303.

General synthetic procedure to obtain aurones (4a–4h)

To a solution of chalcone **3a–h** (1 mmol) in pyridine (10 mL) was added $Hg(OAc)_2$ (1 mmol) at room temperature, and the mixture was refluxed for 2 h. The cooled reaction mixture was poured into ice-cold water (50 mL) and acidified with dil. HCl. The precipitated solid was filtered, washed with cold water, and dried to give the products, which were purified by flash column chromatography using $CHCl_3$ as eluent. In this way, the following aurones were prepared.

(Z)-2-(2,5-Dimethoxybenzylidene)-4-methoxybenzofuran-3(2H)-one (4a)

Yellow solid, yield 80%, mp: 187.4–188.2 °C. ^1H NMR (400 MHz, $CDCl_3$) δ ppm: 3.84 (d, J = 2.6 Hz, 6H), 3.99 (s, 3H), 6.59 (d, J = 8.3 Hz, 1H), 6.82–6.85 (m, 2H), 6.90 (dd, J = 2.8, 9.0 Hz, 1H), 7.34 (s, 1H), 7.53 (t, J = 8.2 Hz, 1H), 7.84 (d, J = 2.8 Hz, 1H). ^{13}C NMR (50 MHz; $CDCl_3$) δ ppm: 55.8, 56.1, 56.2, 104.8, 105.1, 105.9, 111.0, 111.7, 116.4, 116.9, 122.1, 138.1, 147.0, 153.3, 153.4, 158.5, 166.8, 182.2. IR (KBr, cm^{-1}): 1697, 1600, 1252, 1232, 1073. MS (ESI): 313.0 ($C_{18}H_{16}O_5$ $[M + H]^+$). HRMS-ES (m/z): $[M + H]^+$ calcd for $C_{18}H_{16}O_5$, 312.0998; found, 313.1067.

(Z)-2-(2,4,5-Trimethoxybenzylidene)-4-methoxybenzofuran-3(2H)-one (4b)

Orange solid, yield 70%, mp: 173.0–174.3 °C. ^1H NMR (400 MHz, $CDCl_3$) δ *ppm*: 3.76 (s, 3H), 3.83 (s, 3H), 3.88

(s, 6H), 6.43 (s, 1H), 7.10–7.17 (m, 3H), 7.36 (s, 1H), 7.82 (s, 1H). ^{13}C NMR (101 MHz; $CDCl_3$) δ ppm: 55.9, 56.0, 56.4, 56.6, 96.3, 105.1, 108.0, 113.2, 113.6, 114.6, 122.3, 125.5, 143.2, 146.5, 152.3, 155.2, 155.9, 160.5, 184.4. IR (KBr, cm^{-1}):1696, 1595, 1254, 1229, 1215, 1080. MS (ESI): 343.0 ($C_{19}H_{20}O_6$ $[M + H]^+$).

(Z)-2-(2,3-Dimethoxybenzylidene)-4-methoxybenzofuran-3(2H)-one (4c)

Yellow solid, yield 60%, mp: 142.6–148.0 °C. ^{1}H NMR (400 MHz, $CDCl_3$) δ ppm: 3.89 (s, 3H), 3.91 (s, 3H), 3.99 (s, 3H), 6.60 (d, J = 8.3 Hz, 1H), 6.85 (d, J = 8.3 Hz, 1H), 6.95 (d, J = 8.1 Hz, 1H), 7.14 (t, J = 8.1 Hz, 1H), 7.29 (s, 1H), 7.55 (t, J = 8.3 Hz 1H), 7.88 (d, J = 8.0 Hz 1H). ^{13}C NMR (101 MHz; $CDCl_3$) δ ppm: 55.9, 56.3, 61.7, 104.7, 105.2, 105.9, 110.9, 113.8, 123.3, 124.1, 126.7, 138.3, 147.5, 149.2, 152.8, 158.6, 167.0, 182.3. IR (KBr, cm^{-1}): 1704, 1599, 1252, 1077. MS (ESI): 312.0 ($C_{18}H_{16}O_5$ $[M + H]^+$). HRMS-ES (m/z): $[M + H]^+$ calcd for $C_{18}H_{16}O_5$, 312.0998; found, 313.1061.

(Z)-2-(4-Bromo-2,5-dimethoxybenzylidene)-4-methoxybenzofuran-3(2H)-one (4d)

Yellow solid, yield 99%, mp: 129.8–130.7 °C. ^{1}H NMR (400 MHz, $CDCl_3$) δ ppm: 3.86 (s, 3H), 3.95 (s, 3H), 4.00 (s, 3H), 6.61 (d, J = 8.3 Hz, 1H), 6.82 (d, J = 8.2 Hz, 1H), 7.10 (s, 1H), 7.27 (s, 1H), 7.55 (t, J = 8.2 Hz,1H), 7.84 (s, 1H). ^{13}C NMR (101 MHz; $CDCl_3$) δ ppm: 56.3, 56.4, 56.9, 104.7, 105.2, 105.3, 111.0, 114.3, 114.7, 116.2, 121.2, 138.2, 147.0, 150.1, 153.4, 158.6, 166.6, 182.0. IR (KBr, cm^{-1}): 1699, 1600, 1494, 1251, 1215, 1076. HRMS-ES (m/z): $[M + H]^+$ calcd for $C_{18}H_{15}O_5Br$, 390.0103; found, 391.0168.

(Z)-2-(2,5-Dimethoxybenzylidene)-5-methoxybenzofuran-3(2H)-one (4e)

Yellow solid, yield 87%, mp: 154.5–157.8 °C. ^{1}H NMR (400 MHz, $CDCl_3$) δ ppm: 3.86 (s, 6H), 4.00 (s, 3H), 6.85 (d, J = 9.0 Hz, 1H), 6.93 (dd, J = 3.1, 9.0 Hz, 1H), 7.08–7.17 (m, 2H), 7.38 (dd, J = 1.8, 6.9 Hz, 1H), 7.46 (s, 1H), 7.95 (d, J = 3.0 Hz, 1H). ^{13}C NMR (101 MHz; $CDCl_3$) δ ppm: 55.7, 56.2, 56.5, 107.7, 111.9, 115.9, 116.4, 117.7, 118.7, 121.8, 123.3, 123.8, 146.0, 146.9, 153.5, 153.7, 155.6, 184.7. IR (KBr, cm^{-1}): 1692, 1643, 1489, 1219, 1032. MS (ESI): 312.0 ($C_{18}H_{16}O_5$ $[M + H]^+$). HRMS-ES (m/z): $[M + H]^+$ calcd for $C_{18}H_{16}O_5$, 312.0998; found, 313.1056.

(Z)-2-(2,4,5-Trimethoxybenzylidene)-5-methoxybenzofuran-3(2H)-one (4f)

Orange solid, yield 82%, mp: 188.8–192.2 °C. ^{1}H NMR (400 MHz, $CDCl_3$) δ *ppm*: 3.83 (s, 3H), 3.90 (s, 3H), 3.95 (s, 6H), 6.50 (s, 1H), 7.18–7.24 (m, 3H), 7.43 (s, 1H), 7.89 (s, 1H). ^{13}C NMR (101 MHz; $CDCl_3$) δ ppm: 55.9, 56.0, 56.4, 56.6, 96.3, 105.1, 108.0, 113.2, 113.6, 114.6, 122.3, 125.5, 143.2, 146.5, 152.3, 155.2, 155.9, 160.5, 184.4 IR (KBr, cm^{-1}): 1694, 1591, 1488, 1272, 1213, 1194, 1028. HRMS-ES (m/z): $[M + H]^+$ calcd for $C_{19}H_{18}O_6$, 342.1103; found, 343.3533.

(Z)-2-(2,3-Dimethoxybenzylidene)-5-methoxybenzofuran-3(2H)-one (4g)

Yellow solid, yield 99%, mp: 170.8–172.3 °C. ^{1}H NMR (400 MHz, $CDCl_3$) δ ppm: 3.83 (s, 3H), 3.89 (s, 3H), 3.92 (s, 3H), 6.97 (d, J = 8.0 Hz, 1H), 7.15 (t, J = 8.1 Hz, 1H), 7.19–7.26 (m, 3H), 7.35 (s, 1H), 7.91 (d, J = 7.9 Hz, 1H). ^{13}C NMR (101 MHz; $CDCl_3$) δ ppm: 55.9, 56.0, 61.7, 105.3, 107.1, 113.7, 114.1, 121.8, 123.5, 124.2, 126.1, 126.6, 148.3, 149.3, 152.8, 156.1, 161.2, 184.9. IR (KBr, cm^{-1}): 1695, 1645, 1490, 1273, 1115. MS (ESI): 312.0 ($C_{18}H_{16}O_5$ $[M + H]^+$). HRMS-ES (m/z): $[M + H]^+$ calcd for $C_{18}H_{16}O_5$, 312.0998; found, 313.1058.

(Z)-2-(4-Bromo-2,5-dimethoxybenzylidene)-5-methoxybenzofuran-3(2H)-one (4h)

Yellow solid, yield 70%, mp: 169.4–174.6 °C. ^{1}H NMR (400 MHz, $CDCl_3$) δ ppm: 3.84 (s, 3H), 3.86 (d, J = 2.0 Hz, 6H), 6.85 (d, J = 9.0 Hz, 1H), 6.93 (dd, J = 3.0, 9.0 Hz, 1H), 7.23 (b.s, 2H), 7.42 (s, 1H), 7.87 (d, J = 3.0 Hz, 1H). ^{13}C NMR (101 MHz; $CDCl_3$) δ ppm: 56.2, 56.4, 56.6, 105.7, 107.6, 112.1, 114.2, 117.2, 117.5, 122.3, 122.4, 126.4, 148.2, 153.9, 154.0, 156.4, 161.4, 185.2. IR (KBr, cm^{-1}): 1691, 1641, 1593, 1490, 1281, 1233, 1098. MS (ESI): 392.0 ($C_{18}H_{15}O_5$ $[M + H]^+$).

Monoamine oxidase inhibition

All compounds were evaluated as previously described (40). Briefly, a crude rat brain mitochondrial suspension (male Sprague–Dawley rats weighing 180–220 g, killed by decapitation) was used as protein source. Serotonin (5-HT, 100 μM) and 4-dimethylaminophenethylamine (DMAPEA, 5 μM) were used as selective substrates for MAO-A and MAO-B, respectively. The reaction mixtures were analyzed with a Merck-Hitachi HPLC (Tokyo, Japan), employing a C18 reverse phase column (Lichrospher 250 × 4.6 mm, 5 μm) and an amperometric detector (Merck–Recipe L3500A). Tetrahydrofuran and acetonitrile (Merck) were used as eluents. IC_{50} values were determined using Prism Graph Pad software, from plots of inhibition percentages (calculated in relation to a sample of the enzyme treated under the same conditions without inhibitors) versus −log inhibitor concentration (from 1 to 100 μM).

In silico evaluation

During decades, computational methodologies such as quantitative structure–activity relationships (QSAR) or molecular modeling (MM) have been useful tools to advance

in the understanding of drug–receptor interactions (41–44). In the present work, 3D-QSAR and docking evaluations were used to rationalize both the experimental results and the structural requirements necessary to design new ligands.

The structures of all evaluated compounds were optimized with Gaussian 03 (45), with the HF–6-31G* method.

Molecular modeling

As the crystal structure of rat MAO-B (rMAO-B) has not been resolved, a homology model was built from the crystallographic data of human MAO-B (PDB: 2V5Z) obtained from the Brookhaven Protein Data Bank for all calculations. The target protein and template were aligned by amino acid identity. MODELLER9v6 (46) was used to construct the three-dimensional structure using standard parameters, and the outputs were ranked on the basis of the internal scoring function of the program. The best model was submitted to the H++ server (47,48) to compute pK values of ionizable groups in the protein and to add missing hydrogen atoms according to the specified pH of the environment. The protein was then inserted into a POPC membrane, TIP3 solvated, and ions were added creating an overall neutral system in approximately 0.1 M NaCl. The ions were equally distributed in a water box. The final system was submitted to a molecular dynamics (MD) simulation for 2 ns using the CHARMM31 force field and the NAMD 2.6 program (49).

The NPT ensemble was used to perform MD calculations. Periodic boundary conditions were applied to the system in the three co-ordinate directions. For non-bonded calculations, a cutoff of 12 Å was used. The long-range electrostatics was calculated using the particle mesh Ewald (PME) method. A pressure of 1 atm was used, and the temperature was kept at 310 K. The evaluation of the structure involved analysis of geometry, stereochemistry, and energy distribution with the VMD program (50), PROSAII server (51), ANOLEA server (52) and Procheck (53).

Molecular docking

Docking studies employed AutoDock Vina software (54) considering the protein to be rigid with flexible ligands. The volume chosen for the grid box was 20 $Å^3$, centered on N5 of the FAD cofactor located in the ligand-binding site. The docked compound complexes were built using the lowest free-energy binding positions. The binding energies

Table 1: Inhibition percentage (IP) of isoforms of rMAO by the synthesized chalcones and aurones, in 10 μM concentrations

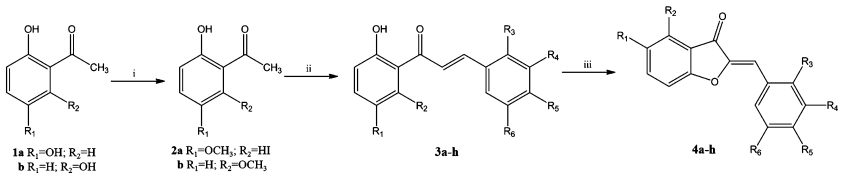

Compound	R_1	R_2	R_3	R_4	R_5	IP(%) of rMAO-A	IP(%) of rMAO-B
3a	H	OCH_3	H	H	OCH_3	0	64
3b	H	OCH_3	H	OCH_3	OCH_3	0	62
3c	H	OCH_3	OCH_3	H	H	14	58
3d	H	OCH_3	H	Br	OCH_3	32	66
3e	OCH_3	H	H	H	OCH_3	2	49
3f	OCH_3	H	H	OCH_3	OCH_3	11	58
3g	OCH_3	H	OCH_3	H	H	23	71
3h	OCH_3	H	H	Br	OCH_3	34	60
4a	H	OCH_3	H	H	OCH_3	23	57
4b	H	OCH_3	H	OCH_3	OCH_3	8	48
4c	H	OCH_3	OCH_3	H	H	0	54
4d	H	OCH_3	H	Br	OCH_3	16	60
4e	OCH_3	H	H	H	OCH_3	11	61
4f	OCH_3	H	H	OCH_3	OCH_3	16	58
4g	OCH_3	H	OCH_3	H	H	0	68
4 h	OCH_3	H	H	Br	OCH_3	0	72

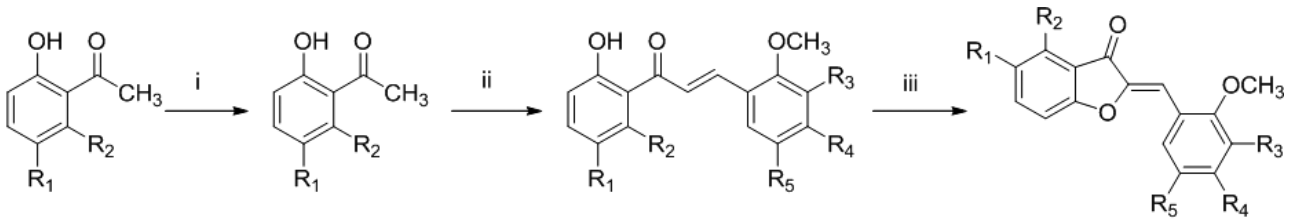

Scheme 1: Reagents and conditions: (i) MeI, acetone, 12 h; rt (ii) ArCHO, EtOH, KOH 50%, 12 h, rt, 34–99%; (iii) $Hg(OAc)_2$, Py, reflux, 2 h, 60–99%. For compounds **3a**–**h** and **4a**–**h**, the substituents R_1–R_5 are indicated in Table 1.

in AutoDock Vina are determined using the AMBER force field. The main interactions were identified using the VMD program (50).

3D-QSAR studies

The pharmacophore models were developed for rat MAO-B (rMAO-B) inhibitors using the phase 3.4 (55) module implemented in the Maestro modeling package (Schrödinger, Inc., LLC, New York, NY, USA). The ligands were prepared in LigPrep module at pH 7. Conformer generation was carried out using MacroModel with the force field OPLS_2005. The solvent model was used with distance-dependent dielectric. The pharmacophores were defined with a root mean square deviation (RMSD) lower than 1 Å. The pharmacophore features for the molecules applying a set of features defined in phase that include hydrogen bond acceptor (A), hydrogen bond donor (D), hydrophobic moiety (H), negative group (N), positive group (P) and aromatic ring (R). Based on the experimental data, the compounds with $IC_{50} \leq 12$ μM ($pIC_{50} \geq -1.08$) were considered as active, while those with $IC_{50} \geq 13$ μM ($pIC_{50} \leq -1.11$) as inactive. Hypotheses were obtained for variation of number of sites and the number of matching active compounds (from 5 to 3). The common pharmacophore was obtained using four sites that matched in the active ligands. Active and inactive molecules were then scored for a given pharmacophore using default parameters: 1 for site, volume, vector, selectivity, and 1.1 for number of matches. Top ranking hypotheses were subjected to 3D-QSAR analysis for which grid spacing was 1 Å and maximum PLS factors 1.

Results and Discussion

The preparation of the chalcones and aurones listed in Table 1 is described in Scheme 1 (56). 2-Hydroxy-5- or -6-methoxyacetophenone (**2a**–**b**) was obtained by regioselective alkylation of the respective dihydroxyacetophenone **1a**–**b** (38) and treated with various substituted benzaldehydes in ethanolic KOH to give chalcones **3a**–**h**. Preparation of the corresponding aurones by oxidative cyclization of the obtained chalcones was achieved by a modification of a reported procedure. Sekizaki described a preparation of aurones from chalcones by treatment with mercury (II) acetate in acetic acid, but flavanones were a by-product in these reactions (57). We employed mercury (II) acetate in pyridine, obtaining only aurones **4a**–**h** in good yields (58). In all cases, a single geometric isomer (*Z*) was obtained as confirmed by analysis of the ^1H and ^{13}C NMR spectra, which were in agreement with previously reported data.

Evaluation of chalcones and aurones as MAO inhibitors

Prior to a complete evaluation of the potential MAOi activity of all chalcones and aurones studied in this work, a preliminary screening of all compounds was carried out for rat MAO-A and MAO-B. The inhibition percentages of isoform B by 10 μM solutions of chalcones **3a**–**h** and aurones **4a**–**h** are listed in Table 1.

All compounds exhibited some degree of selectivity as MAO-B inhibitors, showing little or no activity vis-à-vis MAO-A. This selectivity of chalcones has been reported by different groups before and, aurones seem to follow the same trend.

These preliminary observations reveal some interesting structural features regarding the activity of these com-

Table 2: IC_{50} values for chalcones and aurones with higher activity as rMAO-B inhibitors

	IC_{50} (μM)[a]		
Compound	MAO-A	MAO-B	Selectivity index (SI)[b]
3a	>100	10.9 ± 0.0	>9.2
3d	>100	6.1 ± 0.1	>16.4
3g	>100	6.8 ± 2.1	>14.7
3h	>100	2.8 ± 0.2	>35.7
4a	>100	17.8 ± 0.3	>5.6
4d	>100	26.3 ± 0.3	>3.8
4g	>100	11.6 ± 0.2	>8.6
4h	>100	13.5 ± 0.0	>7.4

[a]IC_{50} values are determined in triplicate in the range of 1–100 μM.
[b]Selectivity Index: expressed as the ratio IC_{50} (MAO-A) / IC_{50} (MAO-B).

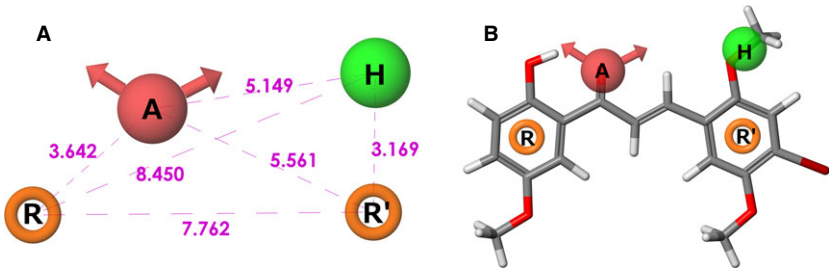

Figure 2: (A) Pharmacophoric landscapes; (B) Superimposition of these features on the structure of **3h**.

pounds as MAO-B inhibitors. Thus, irrespective of the substitution pattern of ring B, the inhibitory activity of all the compounds was stronger when $R_2 = OCH_3$ on ring A, than when $R_1 = OCH_3$. The only exception to this was the pair **3c**/**3g**. Bromination of ring B at R_3 also seemed to improve the inhibitory activity of the chalcone/aurone, as can be seen by a comparison of pair **3e/h** and **4e/h**. Then, we evaluated in more detail the best inhibitors of the two sets considering the substitution pattern. The obtained IC_{50} values of compounds **3a**, **3d**, **3g**, **3h**, **4a**, **4d**, **4g**, and **4h** as MAO-B inhibitors and their selectivity indexes are listed in Table 2.

Analysis of the data of Table 2 shows that chalcones (**3**) are in general more active than the corresponding aurones (**4**). As discussed below, this may be related with the fact that cyclization in the latter compounds eliminates the possibility of establishing hydrogen bonds between amino acid residues in the active site of MAO-B and a hydroxyl substituent on ring A. Of all the compounds, chalcone **3h** was the best MAO-B inhibitor, with an IC_{50} of 2.8 μM. Interestingly, compound **3h** exhibited both structural features mentioned above, an adequate substitution pattern on ring A and a brominated ring B.

Table 3: Experimental and predicted IC_{50} values of training set compounds based on 3D-QSAR hypothesis

Compound	Experimental pIC_{50} (μM)	Calculated pIC_{50} (μM)
3a	−1.03	−0.86
3d	−0.78	−0.82
3g	−0.83	−0.72
3h	−0.45	−0.65
4a	−1.28	−1.34
4d	−1.41	−1.34
4g	−1.06	−1.17
4h	−1.13	−1.27

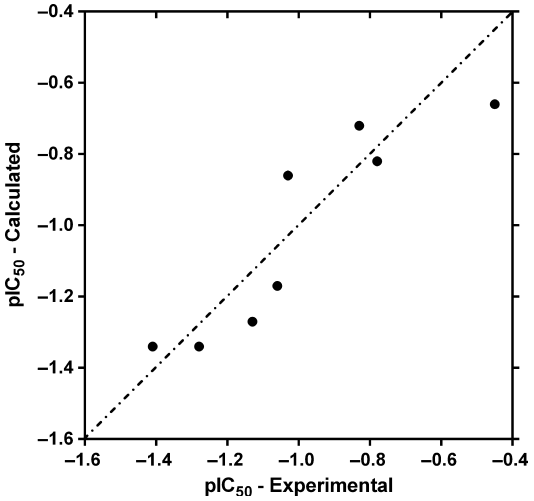

Figure 3: Plot of predicted versus experimental pIC_{50} values for the QSAR model applied to the chalcones and aurones of Table 3. The dashed line shows the linear fit for the theoretical versus the experimental values, with a correlation coefficient $r^2 = 0.822$ and a standard deviation of 0.16.

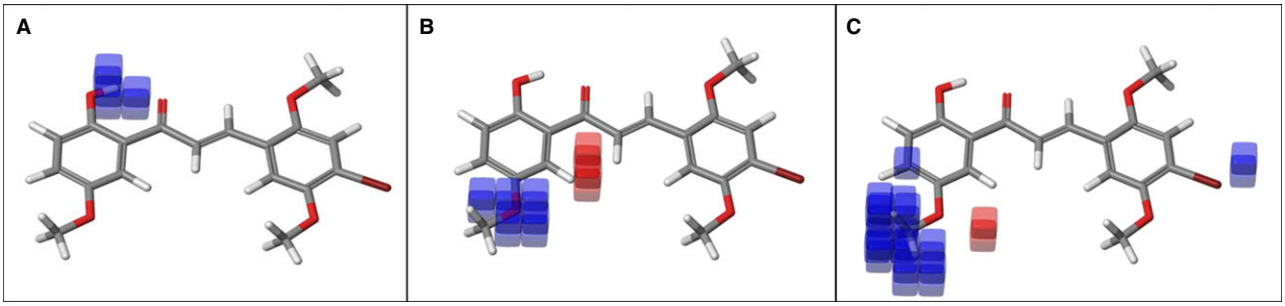

Figure 4: Combined effect from 3D-QSAR hypotheses. Visualization of substituents effect: blue cubes showing positive potential while red cubes showing negative potential of (A) hydrogen bond donor, (B) electron-withdrawing feature, and (C) hydrophobic features.

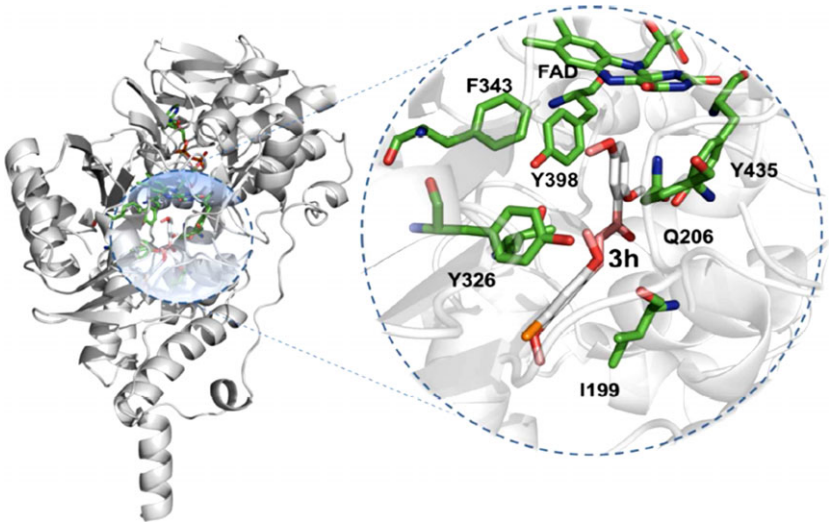

Figure 5: Binding mode of **3h** (White) inside of the active site of hMAO-B. The amino acid residues lining the active site of MAO-B are displayed in green.

Our results are in agreement with previous reports where chalcone derivatives prepared by Chimenti *et al.* (23), and Desideri *et al.* (59), showed a similar pattern, in which an OH group as R_1 and an OCH_3 as R_3, and a halogen atom as R_4' led to the highest inhibitory activity.

Computational

3D-QSAR studies

As an attempt to identify a common pharmacophore conferring the MAO-B inhibitory properties, a 3D-QSAR study was carried out.

The set of 8 compounds selected as the most active MAO-B inhibitors was then subjected to a three-dimensional structure–activity relationship (3D-QSAR) study, aimed to find the structural features responsible for their activity. This approach allowed us to relate quantitatively, by means of a partial least squares regression, three-dimensional descriptors with the measured IC_{50} values of the studied compounds. Inspection of the structures revealed pharmacophoric features that might be responsible for their activity, and which were adopted as a starting hypothesis in the search of relevant 3D descriptors. These features included hydrogen-bond-accepting (A) groups, two aromatic groups (R), and hydrophobic substituents (H). Figure 2A describes the pharmacophoric features present in the set, with the distances in Å between each pair. Figure 2B depicts these features, as applied to the structure of **3h**, the best inhibitor of the set.

The best regression taking into account these features led to predicted pIC_{50} values that correlated with the corresponding experimental values listed in Table 3, with a correlation coefficient $R^2 = 0.822$. Figure 3 is a plot of these data.

A pictorial description of the best regression obtained is shown in Figure 4, for compound **3h**. Blue pharmacophoric features correspond to positive contributions to the activity, whereas negative ones are represented in red. Thus, for compound **3h**, these features include a hydroxyl substituent on ring A, capable of forming a hydrogen bond with the carbonyl group; a second hydrogen-bond-accepting methoxy group on ring A, *para* to the OH substituent, and a hydrophobic Br substituent on ring B.

Docking studies

We next employed molecular mechanics studies to search for interactions within the active site of MAO-B that might support the 3D-QSAR picture developed in the previous

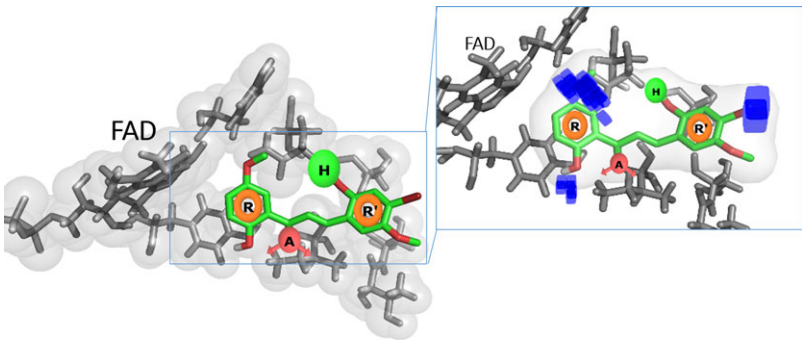

Figure 6: Superimposition of the structure of chalcone **3h** (green), docked into the active site of hMAO-B (amino acids are displayed in cyan), with the main pharmacophoric features of this inhibitor, obtained from the 3D-QSAR studies.

section. The active site of MAO-B is formed by an entrance and a binding cavity, with aromatic amino acid residues aligned in such a way those inhibitors with long, planar ring systems, capable of developing π–π interactions with these residues are well accommodated within the site. This may be the reason why chalcones and aurones are selective MAO-B inhibitors, and are less active vis-à-vis MAO-A, which does not possess an active site with these characteristics (60). The MAO-B binding site includes a pair of tyrosines (Y435 and Y398) close to the FAD cofactor, which should also be capable of forming π–π interactions with an electron-poor aromatic ring. This may also be the reason why the aromatic ring A of chalcones is preferentially situated close to the isoalloxazine molecule. In the case of the less active aurones, our docking studies revealed the opposite situation, with ring B positioned close to the FAD fragment. This is probably a consequence of the lack of coplanarity of rings A and B in aurones, forcing the molecule to locate the aromatics centers perpendicularly between them, within the active site of the enzyme. In fact, optimization of all the aurone structures investigated in these docking studies led to an average dihedral angle of 125° between the two rings. When this planarity is maintained, as in all investigated chalcones (with an average dihedral angle of 180°), ring A locates close to the FAD cofactor. Docking of the most active aurones and chalcones of the series led in all cases to final stable conformations which illustrate the points mentioned above. Thus, for the most active member of the series, chalcone **3h**, ring A is positioned close to the FAD fragment and flanked by Y435 and Y398 (Figure 5).

The 4-methoxy substituent on ring A is also capable of forming hydrogen bonds with the glutamine residue Q206, in agreement with our 3D-QSAR results of the previous section, which identified it as an important positive pharmacophoric feature. As both binding and entrance cavities of the active site have non-polar character, it is not surprising that increasing the lipophilicity of ring B with the large 4-bromo substituent, as in **3h**, has the result of favoring insertion of this ring into the entrance cavity. Thus, the major pharmacophoric features responsible for the increased MAO-B inhibitory activity of chalcones and aurones listed in Table 3 find some correlation with docking studies carried out with these compounds in the active site of the enzyme. This general conclusion is graphically illustrated by Figure 6, where the most active MAO-B inhibitor, chalcone **3h**, is depicted inside the enzyme active site, with its main pharmacophoric features highlighted.

Conclusions

Our findings show that chalcones and aurones are moderately selective inhibitors of MAO-B and have potential as versatile non-nitrogenous scaffolds. Our present study employing molecular modeling methodologies, docking, and structure–activity relationships led to the identification of possible structural modifications to generate more and/or better interactions of these compounds with the MAO-B isoform, thereby increasing the activity and selectivity of these compounds as MAO-B inhibitors. Our suggested modifications await the future synthesis and evaluation of novel aurones and chalcones as MAO-B inhibitors, a goal which is beyond the scope of the present work.

Acknowledgments

This work was supported by FONDECYT (Research Grant) No. 1090037 (AF), 1130185 (MR-P), and 1120128 (COS).

References

1. Roman B.I., Heugebaert T.S., Bracke M.E., Stevens C.V. (2013) Assessment of the antineoplastic potential of chalcones in animal models. Curr Med Chem;20:186–221.
2. Detsi A., Majdalani M., Kontogiorgis C.A., Hadjipavlou-Litina D., Kefalas P. (2009) Natural and synthetic 2′-hydroxy-chalcones and aurones: synthesis, characterization and evaluation of the antioxidant and soybean lipoxygenase inhibitory activity. Bioorg Med Chem;17:8073–8085.
3. Hadjeri M., Beney C., Boumendjel A. (2003) Recent advances in the synthesis of conveniently substituted flavones, quinolones, chalcones and aurones: potential biologically active molecules. Curr Org Chem;7:679–689.
4. Bhasker N., Reddy M.K. (2011) Synthesis and antibacterial activity of prenyloxy chalcones and prenyloxy aurones. Indian J Heterocycl Chem;21:49–52.
5. Tiwari K.N., Monserrat J.P., Hequet A., Ganem-Elbaz C., Cresteil T., Jaouen G., Vessieres A. *et al.* (2012) In vitro inhibitory properties of ferrocene-substituted chalcones and aurones on bacterial and human cell cultures. Dalton Trans;41:6451–6457.
6. Zwergel C., Gaascht F., Valente S., Diederich M., Bagrel D., Kirsch G. (2012) Aurones: interesting natural and synthetic compounds with emerging biological potential. Nat Prod Commun;7:389–394.
7. Haudecoeur R., Boumendjel A. (2012) Recent advances in the medicinal chemistry of aurones. Curr Med Chem;19:2861–2875.
8. Kim S.Y., Lee I.S., Moon A. (2013) 2-Hydroxychalcone and xanthohumol inhibit invasion of triple negative breast cancer cells. Chem Biol Interact;203:565–572.
9. Blanquer-Rossello M.M., Oliver J., Valle A., Roca P. (2013) Effect of xanthohumol and 8-prenylnaringenin on MCF-7 breast cancer cells oxidative stress and mitochondrial complexes expression. J Cell Biochem;114:2785–2794.
10. Wyns C., van Steendam K., Vanhoecke B., Deforce D., Bracke M., Heyerick A. (2012) Prenylated chalcone

xanthohumol associates with histones in breast cancer cells–a novel target identified by a monoclonal antibody. Mol Nutr Food Res;56:1688–1696.
11. Liu Y., Gao X., Deeb D., Arbab A.S., Dulchavsky S.A., Gautam S.C. (2012) Anticancer agent xanthohumol inhibits IL-2 induced signaling pathways involved in T cell proliferation. J Exp Ther Oncol;10:1–8.
12. Magalhaes P.J., Carvalho D.O., Cruz J.M., Guido L.F., Barros A.A. (2009) Fundamentals and health benefits of xanthohumol, a natural product derived from hops and beer. Nat Prod Commun;4:591–610.
13. Park S., Gwak J., Han S.J., Oh S. (2013) Cardamonin suppresses the proliferation of colon cancer cells by promoting beta-catenin degradation. Biol Pharm Bull;36:1040–1044.
14. Dzoyem J.P., Hamamoto H., Ngameni B., Ngadjui B.T., Sekimizu K. (2013) Antimicrobial action mechanism of flavonoids from *Dorstenia* species. Drug Discov Ther;7:66–72.
15. Lee Y.M., Hsieh K.H., Lu W.J., Chou H.C., Chou D.S., Lien L.M., Sheu J.R., Lin K.H. (2012) Xanthohumol, a prenylated flavonoid from hops (*Humulus lupulus*), prevents platelet activation in human platelets. Evid Based Complement Alternat Med;2012:852362.
16. Lee D.S., Jeong G.S., Li B., Park H., Kim Y.C. (2010) Anti-inflammatory effects of sulfuretin from *Rhus verniciflua* stokes via the induction of heme oxygenase-1 expression in murine macrophages. Int Immunopharmacol;10:850–858.
17. Shin J.S., Park Y.M., Choi J.H., Park H.J., Shin M.C., Lee Y.S., Lee K.T. (2010) Sulfuretin isolated from heartwood of *Rhus verniciflua* inhibits LPS-induced inducible nitric oxide synthase, cyclooxygenase-2, and pro-inflammatory cytokines expression via the down-regulation of NF-kappaB in RAW 264.7 murine macrophage cells. Int Immunopharmacol;10:943–950.
18. Song M.Y., Jeong G.S., Lee H.S., Kwon K.S., Lee S.M., Park J.W., Kim Y.C., Park B.H. (2010) Sulfuretin attenuates allergic airway inflammation in mice. Biochem Biophys Res Commun;400:83–88.
19. Poudel S., Song J., Jin E.J., Song K. (2013) Sulfuretin-induced miR-30C selectively downregulates cyclin D1 and D2 and triggers cell death in human cancer cell lines. Biochem Biophys Res Commun;431:572–578.
20. Kim J.M., Noh E.M., Kwon K.B., Kim J.S., You Y.O., Hwang J.K., Hwang B.M., Kim M.S., Lee S.J., Jung S.H., Youn H.J., Chung E.Y., Lee Y.R. (2013) Suppression of TPA-induced tumor cell invasion by sulfuretin via inhibition of NF-kappaB-dependent MMP-9 expression. Oncol Rep;29:1231–1237.
21. Kumar K.S., Kumaresan R. (2011) A quantum chemical study on the antioxidant properties of aureusidin and bracteatin. Int J Quantum Chem;111:4483–4496.
22. Siddaiah V., Maheswara M., Venkata Rao C., Venkateswarlu S., Subbaraju G.V. (2007) Synthesis, structural revision, and antioxidant activities of antimutagenic homoisoflavonoids from *Hoffmanosseggia intricata*. Bioorg Med Chem Lett;17:1288–1290.
23. Chimenti F., Fioravanti R., Bolasco A., Chimenti P., Secci D., Rossi F., Yáñez M., Orallo F., Ortuso F., Alcaro S. (2009) Chalcones: a valid scaffold for monoamine oxidases inhibitors. J Med Chem;52:2818–2824.
24. Jo G., Ahn S., Kim B.G., Park H.R., Kim Y.H., Choo H.A., Koh D., Chong Y., Ahn J.H., Lim Y. (2013) Chromenylchalcones with inhibitory effects on monoamine oxidase B. Bioorg Med Chem;21:7890–7897.
25. Robinson S.J., Petzer J.P., Petzer A., Bergh J.J., Lourens A.C.U. (2013) Selected furanochalcones as inhibitors of monoamine oxidase. Bioorg Med Chem Lett;23:4985–4989.
26. Finberg J.P. (2014) Update on the pharmacology of selective inhibitors of MAO-A and MAO-B: focus on modulation of CNS monoamine neurotransmitter release. Pharmacol Ther;143:133–152.
27. Edmondson D.E., Binda C., Mattevi A. (2007) Structural insights into the mechanism of amine oxidation by monoamine oxidases A and B. Arch Biochem Biophys;464:269–276.
28. Johnston J.P. (1968) Some observations upon a new inhibitor of monoamine oxidase in brain tissue. Biochem Pharmacol;17:1285–1297.
29. Edmondson D.E., Binda C., Wang J., Upadhyay A.K., Mattevi A. (2009) Molecular and mechanistic properties of the membrane-bound mitochondrial monoamine oxidases. Biochemistry;48:4220–4230.
30. Upadhyay A.K., Borbat P.P., Wang J., Freed J.H., Edmondson D.E. (2008) Determination of the oligomeric states of human and rat monoamine oxidases in the outer mitochondrial membrane and octyl beta-D-glucopyranoside micelles using pulsed dipolar electron spin resonance spectroscopy. Biochemistry;47:1554–1566.
31. Bonnet U. (2003) Moclobemide: therapeutic use and clinical studies. CNS Drug Rev;9:97–140.
32. Song M.S., Matveychuk D., MacKenzie E.M., Duchcherer M., Mousseau D.D., Baker G.B. (2013) An update on amine oxidase inhibitors: multifaceted drugs. Progr Neuropsychopharmacol Biol Psychiatry;44:118–124.
33. Nicotra A., Pierucci F., Parvez H., Senatori O. (2004) Monoamine oxidase expression during development and aging. Neurotoxicology;25:155–165.
34. Fowler J.S., Volkow N.D., Wang G.J., Logan J., Pappas N., Shea C., MacGregor R. (1997) Age-related increases in brain monoamine oxidase B in living healthy human subjects. Neurobiol Aging;18:431–435.
35. Legoabe L.J., Petzer A., Petzer J.P. (2014) Alpha-Tetralone derivatives as inhibitors of monoamine oxidase. Bioorg Med Chem Lett;24:2758–2763.
36. Neudorfer C., Shanab K., Jurik A., Schreiber V., Neudorfer C., Vraka C., Schirmer E., Holzer W., Ecker G., Mitterhauser M., Wadsak W., Spreitzer H. (2014) Development of potential selective and reversible pyrazoline based MAO-B inhibitors as MAO-B PET tracer precursors and reference substances for the early

detection of Alzheimer's disease. Bioorg Med Chem Lett;24:4490–4495.
37. Salgin-Goksen U., Yabanoglu-Ciftci S., Ercan A., Yelekci K., Ucar G., Gokhan-Kelekci N. (2013) Evaluation of selective human MAO inhibitory activities of some novel pyrazoline derivatives. J Neural Transm;120:863–873.
38. Shah G.N., Va N.M. (1951) Quinacetophenone monomethyl ether. Org Synth;31:90–91.
39. Shin S.Y., Jung H., Ahn S., Hwang D., Yoon H., Hyun J., Yong Y., Cho H.J., Koh D., Lee Y.H., Lim Y. (2014) Polyphenols bearing cinnamaldehyde scaffold showing cell growth inhibitory effects on the cisplatin-resistant A2780/Cis ovarian cancer cells. Bioorg Med Chem;22:1809–1820.
40. Fierro A., Osorio-Olivares M., Cassels B.K., Edmondson D.E., Sepulveda-Boza S., Reyes-Parada M. (2007) Human and rat monoamine oxidase-A are differentially inhibited by (S)-4-alkylthioamphetamine derivatives: insights from molecular modeling studies. Bioorg Med Chem;15:5198–5206.
41. Sliwoski G., Kothiwale S., Meiler J., Lowe E.W. Jr (2014) Computational methods in drug discovery. Pharmacol Rev;66:334–395.
42. Chang H.W., Chung F.S., Yang C.N. (2013) Molecular modeling of p38α mitogen-activated protein kinase inhibitors through 3D-QSAR and molecular dynamics simulations. J Chem Inf Mod;53:1775–1786.
43. Fontes Ferreira da Cunha E., Albuquerque M.G., Ceva Antunes O.A., Bicca de Alencastro R. (2005) 4D-QSAR models of HOE/BAY-793 analogues as HIV-1 protease inhibitors. QSAR Comb Sci;24:240–253.
44. Li D., Liu M.S., Ji B., Hwang K.C., Huang Y. (2012) Identifying the molecular mechanics and binding dynamics characteristics of potent inhibitors to HIV-1 protease. Chem Biol Drug Des;80:440–454.
45. Frisch M.J., Trucks G.W., Schlegel H.B., Scuseria G.E., Robb M.A., Cheeseman J.R., Montgomery J.A. *et al.* (2004) Gaussian 03, R. C. Wallingford, CT: Gaussian, Inc.
46. Sali A., Blundell T.L. (1993) Comparative protein modelling by satisfaction of spatial restraints. J Mol Biol;234:779–815.
47. Gordon J.C., Myers J.B., Folta T., Shoja V., Heath L.S., Onufriev A. (2005) H++: a server for estimating pKas and adding missing hydrogens to macromolecules. Nucleic Acids Res;33:W368–W371.
48. 1Anandakrishnan R., Onufriev A. (2008) Analysis of basic clustering algorithms for numerical estimation of statistical averages in biomolecules. J Comput Biol;15:165–184.
49. Phillips J.C., Braun R., Wang W., Gumbart J., Tajkhorshid E., Villa E., Chipot C., Skeel R.D., Kalé L., Schulten K. (2005) Scalable molecular dynamics with NAMD. J Comput Chem;26:1781–1802.
50. Humphrey W., Dalke A., Schulten K. (1996) VMD: visual molecular dynamics. J Mol Graphics;14:33–38, 27-8.
51. Wiederstein M., Sippl M.J. (2007) ProSA-web: interactive web service for the recognition of errors in three-dimensional structures of proteins. Nucleic Acids Res;35:W407–W410.
52. Melo F., Devos D., Depiereux E., Feytmans E. (1997) ANOLEA: a www server to assess protein structures. Proc Int Conf Intell Syst Mol Biol;5:187–190.
53. Laskowski R.A., Macarthur M.W., Moss D.S., Thornton J.M. (1993) Procheck - a program to check the stereochemical quality of protein structures. J Appl Crystallogr;26:283–291.
54. Trott O., Olson A.J. (2010) AutoDock Vina: improving the speed and accuracy of docking with a new scoring function, efficient optimization, and multithreading. J Comput Chem;31:455–461.
55. Dixon S.L., Smondyrev A.M., Knoll E.H., Rao S.N., Shaw D.E., Friesner R.A. (2006) PHASE: a new engine for pharmacophore perception, 3D QSAR model development, and 3D database screening: 1. Methodology and preliminary results. J Comput Aid Mol Des;20:647–671.
56. Venkateswarlu S., Panchagnula G.K., Gottumukkala A.L., Subbaraju G.V. (2007) Synthesis, structural revision, and biological activities of 4 '-chloroaurone, a metabolite of marine brown alga *Spatoglossum variabile*. Tetrahedron;63:6909–6914.
57. Sekizaki H. (1988) Synthesis of 2-benzylidene-3(2h)-Benzofuran-3-Ones (Aurones) by oxidation of 2′-hydroxychalcones with mercury(Ii) acetate. B Chem Soc Jpn;61:1407–1409.
58. Agrawal N.N., Soni P.A. (2006) A new process for the synthesis of aurones by using mercury (II) acetate in pyridine and cupric bromide in dimethyl sulfoxide. Indian J Chem B;45:1301–1303.
59. Desideri N., Bolasco A., Fioravanti R., Monaco L.P., Orallo F., Yanez M., Ortuso F., Alcaro S. (2011) Homoisoflavonoids: natural scaffolds with potent and selective monoamine oxidase-B inhibition properties. J Med Chem;54:2155–2164.
60. Edmondson D.E., Mattevi A., Binda C., Li M., Hubalek F. (2004) Structure and mechanism of monoamine oxidase. Curr Med Chem;11:1983–1993.